

# Multi-Omics Integration with Machine Learning and Molecular Docking Reveals Crosstalk Mechanisms and Drug Candidates in Metastatic Melanoma and Vitiligo

Heng Yang<sup>1,2,\*</sup>, Jiayue Yang<sup>1,3,\*</sup>, Huilan Zheng<sup>1,2</sup>, Yao Dai<sup>4</sup>, Xiqian Chen<sup>5</sup>, Jingping Wu<sup>1,6</sup>, Xiao Ma<sup>7</sup>, Hongbin Cheng<sup>1,2</sup>

<sup>1</sup>School of Clinical Medicine, Chengdu University of Traditional Chinese Medicine, Chengdu, 610075, People's Republic of China; <sup>2</sup>Department of Dermatology, Hospital of Chengdu University of Traditional Chinese Medicine, Chengdu, 610072, People's Republic of China; <sup>3</sup>Department of Rheumatology, Hospital of Chengdu University of Traditional Chinese Medicine, Chengdu, 610072, People's Republic of China; <sup>4</sup>The Fourth Affiliated Hospital of Xinjiang Medical University, Xinjiang Medical University, Urumqi, 830054, People's Republic of China; <sup>5</sup>Department of Dermatology, the Affiliated Hospital of Southwest Medical University, Luzhou, 646000, People's Republic of China; <sup>6</sup>Department of Medical Cosmetology, Hospital of Chengdu University of Traditional Chinese Medicine, Chengdu, 610072, People's Republic of China; <sup>7</sup>School of Pharmacy, Chengdu University of Traditional Chinese Medicine, Chengdu, 611137, People's Republic of China

\*These authors contributed equally to this work

Correspondence: Xiao Ma; Hongbin Cheng, Email tobymaxiao@cdutcm.edu.cn; chenghongbin@cdutcm.edu.cn

**Objective:** The aim of this study was to systematically elucidate the crosstalk mechanisms between metastatic melanoma and vitiligo and to establish vitiligo and metastasis-based biomarkers as well as to find drug candidates.

**Methods:** The genes associated with vitiligo and metastatic melanoma were obtained through differential expression analysis and WGCNA using publicly available data from GEO and TCGA. A prognostic model and nomogram for melanoma were subsequently constructed using hub genes based on machine learning algorithms. A comprehensive assessment was conducted of the correlation between hub genes and overall survival, functional annotations, immune cells and immune checkpoint genes. At the single-cell level, we conducted scoring using the AUCell algorithm and CellChat analysis to facilitate more profound biological exploration. The Cmap database and molecular docking methods were used to screen drug candidates.

**Results:** Following the screening process, a total of six hub genes (*DUOX1*, *GJB3*, *NOTCH3*, *PKP1*, *PTK6* and *PTPRF*) were employed in the construction of prognostic model by machine learning. Patients were stratified into high-risk and low-risk groups based on the model. The expression of hub genes and the predictive ability of the model were validated in independent cohorts. The high-risk group exhibited worse prognosis, greater immunosuppression and tumor-associated macrophage infiltration. A nomogram based on the risk score had great performance in predicting survival of melanoma patients at 1-, 3-, and 5-year time points. The scRNA-seq results indicated that hub genes may exert an influence on tumor progression and metastasis by affecting fibroblasts and thus promoting epithelial-mesenchymal transition. Methyl-angolensate, byssochlamic-acid, homoharringtonine, piperacillin and cephaeline were potentially targeted therapeutic compounds for hub genes based on molecular docking.

**Conclusion:** Our study firstly provides new insight into the genetic crosstalk between metastatic melanoma and vitiligo that may facilitate the development of personalized treatments.

**Keywords:** metastatic melanoma, vitiligo, machine learning, scRNAseq, molecular docking

## Introduction

Melanoma is a malignant tumor of the skin that arises from the malignant proliferation of melanocytes. It is characterized by strong aggressiveness, early metastasis and a poor prognosis.<sup>1</sup> The American Society of Clinical Oncology (ASCO) has observed a notable increase in the incidence and lethality of melanoma over recent decades, with the disease now



representing a significant public health burden.<sup>2</sup> It is widely accepted that sun exposure and ultraviolet radiation (UVR) are significant contributing factors in the development of melanoma.<sup>3</sup> The advent of immune checkpoint inhibitors in conjunction with conventional surgical treatments has enhanced the survival prospects of melanoma patients. However, a proportion of patients remain unresponsive or exhibit drug resistance.<sup>4</sup>

In clinical practice, an association has been identified between vitiligo and melanoma. A nonconcurrent cohort demonstrates a significantly reduced incidence of melanoma in patients with vitiligo, despite the potential for increased exposure to UVR.<sup>5</sup> Additionally, another study finds that individuals with vitiligo exhibited a threefold reduction in the likelihood of developing melanoma.<sup>6</sup> Meanwhile, a meta-analysis indicates that patients with stage III–IV melanoma who have developed vitiligo-like depigmentation as a result of immunotherapy exhibit a two- to four-fold reduction in the risk of disease progression and mortality, respectively, in comparison to those who have not developed this phenomenon.<sup>7</sup> These findings suggest that there may be a protective effect associated with vitiligo in the development of melanoma. Vitiligo is an autoimmune disease characterized by the destruction of melanocytes, which results in the loss of pigmentation in the skin.<sup>8</sup> This mechanism is diametrically opposed to that observed in melanoma, a malignant proliferation of melanocytes. It may represent a potential common mechanism of action for vitiligo and melanoma.

The current research indicates that the correlation between vitiligo and melanoma is believed to be the consequence of an immune response against melanoma and normal melanocytes.<sup>9</sup> For example, autoantibodies isolated from patients with vitiligo have been demonstrated to exert destructive effects on melanoma cells in both *in vitro* and *in vivo*.<sup>10</sup> Nevertheless, comprehensive research elucidating the correlation between vitiligo and melanoma at the genetic expression level remains scarce.

Transcriptomics is a technology that can resolve the dynamics of gene expression and its regulatory mechanisms. However, it is difficult to capture deeper molecular mechanisms from a single omics. Therefore, integrating RNA-seq, scRNA-seq and other multi-omics data for comprehensive analysis is the current trend.<sup>11</sup> Meanwhile, in the face of the resulting large amount of high-dimensional, heterogeneous, and non-linearly correlated data, traditional analysis methods have limited effectiveness. Machine learning algorithms can effectively mine key driving features and construct predictive models from complex multi-omics data, providing precise targets for the development of new diagnostic and therapeutic strategies.<sup>12</sup>

In this study, a range of bioinformatics techniques are employed to identify prognostic-related biomarkers from metastatic melanoma and vitiligo. These biomarkers are then used to construct a prognostic model, a nomogram and predict potential drugs. This study may facilitate the acquisition of novel insights into the clinical management and pathogenesis of melanoma.

## Methods

### Datasets of Melanoma and Vitiligo

In this study, the Gene Expression Omnibus (GEO) database (<https://www.ncbi.nlm.nih.gov/geo/>) and The Cancer Genome Atlas (TCGA) database (<https://portal.gdc.cancer.gov/>) were utilized to obtain gene expression data and clinical information on patients with malignant melanoma and vitiligo. The GSE75819<sup>13</sup> and GSE46517<sup>14</sup> datasets were employed to identify differentially expressed genes (DEGs) and to construct a gene co-expression network associated with vitiligo and metastatic melanoma, respectively. The TCGA-SKCM cohort was used to construct a prognostic model for melanoma patients. And the GSE65904<sup>15</sup> dataset was used for the external validation of the prognostic model.

### Data Processing

The datasets GSE75819, GSE46517, and GSE65904 consist of microarray data. The annotation file provided by the corresponding platform was employed to convert the probe ID to the gene symbol. If multiple probes correspond to the same gene, calculated the average of these probes. The *normalizeBetweenArrays()* function from the “limma”<sup>16</sup> R package was used to perform quantile normalization while log<sub>2</sub> scaling the data to reduce the order of magnitude difference. The TCGA-SKCM cohort was bulk RNAseq data (TPM values) scaled by log<sub>2</sub>(TPM + 1). Samples with overall survival <30 days or missing survival information were removed, resulting in the inclusion of 450 melanoma samples for the construction of the prognostic model.

## Differential Expression Analysis

Differential expression analysis was performed using the “limma” R package to obtain DEGs of vitiligo relative to non-lesional skin and metastatic melanoma relative to primary melanoma from GSE75819 and GSE46517. Screening thresholds were false discovery rate (FDR) < 0.05 and  $|\log_2 \text{fold change}| > 0.585$ . Volcano and heatmap plots were visualized using the “ggplot2” and “pheatmap” R packages.

## Weighted Gene Co-Expression Network Analysis (WGCNA)

To identify the modules and key genes associated with the disease phenotype, WGCNA was performed on GSE75819 and GSE46517 using the “WGCNA” R package. According to the scale-free topology criterion, the best softPowers were obtained using the *pickSoftThreshold()* function. Using the *blockwiseModules()* function, a co-expression network was constructed with the minimum module size set to 300 to obtain modules that were closely related to the disease phenotype. Finally, the genes were filtered from the module based on the criteria of module membership (MM) > 0.8 and gene significance (GS) > 0.5.

## Vitiligo and Metastasis Related Genes (VMRGs) Identification and Functional Enrichment

The VMRGs were derived from the intersection of four gene sets: (1) DEGs obtained from GSE75819; (2) DEGs obtained from GSE46517; (3) vitiligo phenotype genes of GSE75819 obtained by WGCNA; and (4) metastatic melanoma phenotype genes of GSE46517 obtained by WGCNA. Meanwhile, the results of (1) (3) and (2) (4) were taken for intersection to obtain VMRGs. The Venn diagram of gene intersections was visualized using “ggvenn” R package. “clusterProfiler”<sup>17</sup> R package was used to perform functional enrichment analysis (gene ontology (GO) and Kyoto encyclopedia of genes and genomes (KEGG)) on the VMRGs to obtain the major biological terms.

## Screening Biomarkers and Building a Prognostic Model with Machine Learning

The entire TCGA-SKCM cohort was used as the training set, while GSE65904 was used as the external validation set. A univariate Cox regression was initially performed to identify VMRGs that were closely associated with overall survival via the “survival” R package. To minimize the potential bias in target screening, two machine learning algorithms were employed to further screen hub VMRGs. Based on the results of the univariate Cox regression, the least absolute shrinkage and selection operator (LASSO) Cox regression was used to further screen genes associated with prognosis via the “glmnet” R package. Additionally, the random forest (RF) algorithm was also employed to further narrow down the range of prognostically relevant genes via the “randomForest” R package. The hub VMRGs that were identified as significant in the LASSO-Cox and RF screening procedures were incorporated into the construction of the prognostic model. Multivariate Cox regression was employed to ascertain the independent prognostic factors and to develop the prognostic model via the “survival” R package. The risk scores were calculated using the prognostic model, and the optimal cutoff value was determined using the *survminer* R package to differentiate between high-risk and low-risk groups. The following formula was employed for the calculation of risk scores:

$$\text{Risk score} = \sum_{i=1}^n [\text{Coef}(\text{gene}_i) \times \text{Expr}(\text{gene}_i)]$$

The disparity in survival prospects between the various risk groups was evaluated through the application of the Kaplan-Meier (KM) method. The “ggrisk” R package was used to visualize the distribution of risk scores and survival status. The receiver operating characteristic (ROC) curve was plotted for 1-, 3-, and 5-year time points using the “timeROC” R package, and the area under the curve (AUC) was calculated.

## Establishment and Validation of the Nomogram

Univariate and multivariate Cox regression were used to ascertain whether risk scores were independent prognostic factors in comparison to age, sex, T stage, N stage, and M stage. Meanwhile, a nomogram was constructed based on risk scores, age, sex, T stage, N stage, and M stage to predict 1-, 3-, and 5-year time points overall survival of melanoma patients by the “rms” R package. Calibration curve analysis was employed to evaluate the accuracy and calibration of the

nomogram based on the KM method. To assess the clinical value of the nomogram, decision curve analysis (DCA) was conducted via the “ggDCA” R package.

## Gene Set Enrichment Analysis (GSEA)

GSEA<sup>18</sup> is a commonly employed method for determining whether a predefined set of genes exhibits a statistically significant and consistent difference between two biological states. The differential expression analysis between the high-risk and low-risk groups was performed based on  $FDR < 0.05$  and  $|\log_2 \text{fold change}| > 0.585$  via the “limma” R package. The DEGs were subsequently employed for GSEA. The Hallmark gene sets (h.all.v2024.1.Hs.symbols) from the Molecular Signatures Database (MSigDB) (<https://www.gsea-msigdb.org/gsea/msigdb>) were utilized as reference gene sets. GSEA was conducted using the “fgsea” R package, and meaningful enriched pathways were selected based on adjusted p-value  $< 0.05$  and sorted according to normalized enrichment score (NES).

## Assessment of the Immunological Properties in Melanoma

The level of infiltration of 22 different immune cells between high-risk and low-risk groups was assessed using the CIBERSORT<sup>19</sup> method. ESTIMATE was employed to calculate the stromal scores and immune scores between the two groups. The difference in the expression of immune checkpoint genes (ICGs) was also evaluated between the two groups. Pearson correlation analysis was utilized to calculate risk scores as well as the correlation of hub VMRGs with immune cells and ICGs.

## Single-Cell RNA Sequencing (scRNA-Seq) Analysis

The raw data were obtained from three cutaneous melanoma samples from the GSE215120<sup>20</sup> dataset, and the “Seurat” R package was employed for scRNA-seq analysis. To exclude low-quality cells, overlapping multiple cells and dead, senescent cells, cells that met the following criteria were filtered out: the number of genes detected per cell exceeded 5,000 or was below 200, the unique molecular identifier (UMI) was above 20,000, and UMI from the mitochondrial genome was above 15%. The top 2,000 highly variable genes (HVGs) were selected for inclusion in a principal component analysis (PCA) for dimensionality reduction. The optimal number of principal components was selected based on the variance explained plot. Since the data came from three different samples, the “harmony” R package was used to remove batch effects. Single-cell clustering visualization was performed using 2D uniform manifold approximation and projection (UMAP). The “clustree” R package was employed for the purpose of computing the optimal resolution in the UMAP reduction process. Each cluster then was annotated with the well-known cell marker genes. Subsequently, the expression of hub VMRGs was investigated in melanoma single-cell samples. The “irGSEA” R package was employed to calculate the AUCell scores of hub VMRGs. The “CellChat” R package was employed to further elucidate the communication relationships between cells.

## Small-Molecule Compounds Prediction and Molecular Docking

The Connectivity Map (CMap) database (<https://clue.io/>) was used to predict small-molecule compounds with therapeutic effects based on DEGs between high risk and low risk groups. The structures of compounds and proteins were obtained from PubChem (<https://pubchem.ncbi.nlm.nih.gov/>) and RCSB PDB (<https://www.rcsb.org/>) databases, respectively. Preprocessing of proteins such as remove ligands, waters, etc. and visualization of results were performed using PyMol Open-Source v3.0. Subsequently, molecular docking was performed using Dockey v1.0.3<sup>21</sup> to verify the binding performance of compounds and proteins. A binding affinity  $< -5.0$  kcal/mol indicated that the small molecule ligand exhibits favourable binding activity with the receptor protein.

## Statistical Analysis

All analysis was conducted using R software v4.4.1. As previously stated, all R packages employed, and the corresponding statistical methodologies were outlined in the preceding section. A p-value of less than 0.05 was deemed to indicate a statistically significant difference.

## Results

### Vitiligo-Related Features and Functions

The GSE75819 dataset was normalized and processed before differential expression analysis. The sample distributions were visualized using boxplots ([Supplementary Figure S1A](#) and [B](#)) and PCA plots ([Supplementary Figure S1C](#) and [D](#)). The differential expression analysis of the processed samples resulted in 1,881 up-regulated genes and 1,800 down-regulated genes (FDR < 0.05 and  $|\log_2$  fold change| > 0.585). The volcano plot and heatmap were employed to visualize these DEGs ([Figure 1A](#) and [B](#)). The WGCNA, based on the expression data of GSE75819, was performed to identify the key gene modules and genes associated with the vitiligo phenotype. Following clustering of the samples, outliers were identified, and 100 were used as the threshold for their removal. This resulted in the removal of a total of 5 samples ([Supplementary Figure S1E](#) and [F](#)). After the screening process, softPower 3 was identified as the optimal value for the network ([Figure 1C](#)). A total of 10 modules were ultimately clustered in GSE75819 ([Figure 1D](#) and [E](#)), among which the turquoise module exhibited a high correlation with the vitiligo phenotype ( $-0.92$ ,  $p < 0.05$ ; [Figure 1E](#)). Therefore, the turquoise module was selected for further analysis. Genes that satisfied the criteria of MM > 0.8 and GS > 0.5 were considered statistically significant ([Figure 1F](#)), resulting in the identification of 1,819 co-expressed genes associated with the vitiligo phenotype. The intersection of the DEGs and the co-expressed genes was taken, and 1,555 vitiligo-related genes were obtained ([Figure 1G](#)). These genes were analyzed by GO and KEGG. The biological process (BP) was primarily associated with mitochondrial translation, whereas the cellular component (CC) was linked to mitochondrial protein-containing complex. And the molecular function (MF) was associated with the structural constituent of ribosome ([Figure 1H](#)). The KEGG pathway of genes associated with vitiligo was found to be enriched for pathways related to the ribosome and oxidative phosphorylation ([Figure 1I](#)).

### Metastatic Melanoma-Related Features and Functions

Similarly, the GSE46517 dataset processing results were shown in the boxplots ([Supplementary Figure S2A](#) and [B](#)) and PCA plots ([Supplementary Figure S2C](#) and [D](#)). Metastatic melanoma had a total of 1,354 DEGs (FDR < 0.05 and  $|\log_2$  fold change| > 0.585) compared to primary melanoma, with 569 up-regulated and 785 down-regulated. Volcano plot and heatmap were also used to visualize the DEGs ([Figure 2A](#) and [B](#)). A WGCNA was conducted on GSE46517 to identify genes associated with metastatic melanoma. Twenty-two outlier samples were excluded based on a threshold of 110 ([Supplementary Figure S2E](#) and [F](#)), after which 5 was selected as softPower to construct the network ([Figure 2C](#)). A total of 7 modules were clustered in GSE46517 ([Figure 2D](#) and [E](#)), with the brown module being the most relevant to metastatic melanoma ( $-0.86$ ,  $p < 0.05$ ; [Figure 2E](#)). A total of 158 genes in the brown module satisfied the criteria of MM > 0.8 and GS > 0.5 ([Figure 2F](#)) and were consequently considered to be co-expressed genes associated with the metastatic melanoma phenotype. Subsequently, a total of 156 metastatic melanoma-associated genes ([Figure 2G](#)) were obtained after intersection of DEGs and co-expressed genes, which were analyzed by GO and KEGG. GO analyses were primarily concerned with the epidermis and skin development ([Figure 2H](#)). The KEGG analysis definitively showed that metastatic melanoma-associated genes were enriched for only two pathways: Staphylococcus aureus infection and estrogen signaling pathway ([Figure 2I](#)).

### Machine Learning Hub VMRGs Identification and Prognostic Model Construction

Following the intersection of genes associated with both vitiligo and metastatic melanoma, a total of 27 VMRGs were identified ([Figure 3A](#)). To obtain prognostically relevant VMRGs, we conducted a further screening of 18 VMRGs that were significantly associated with overall survival in melanoma by univariate Cox regression in the TCGA-SKCM cohort (HR > 1,  $p < 0.05$ ; [Figure 3B](#)). Subsequently, the genes were screened with two classical machine learning algorithms to enhance reliability and accuracy. Based on the LASSO-Cox regression results, 12 genes were selected ([Figure 3C](#) and [D](#)). In addition, MeanDecreaseAccuracy (MDA) scores in RF revealed the importance of each gene, and we selected the top10 MDA genes ([Figure 3E](#)). The LASSO Cox regression and RF overlapped resulted in a total of 6 hub VMRGs (*DUOX1*, *GJB3*, *NOTCH3*, *PKP1*, *PTK6*, and *PTPRF*). Then, we constructed a prognostic model based on 6 hub VMRGs using multivariate Cox regression. The training set was derived from 450 samples from the TCGA-SKCM

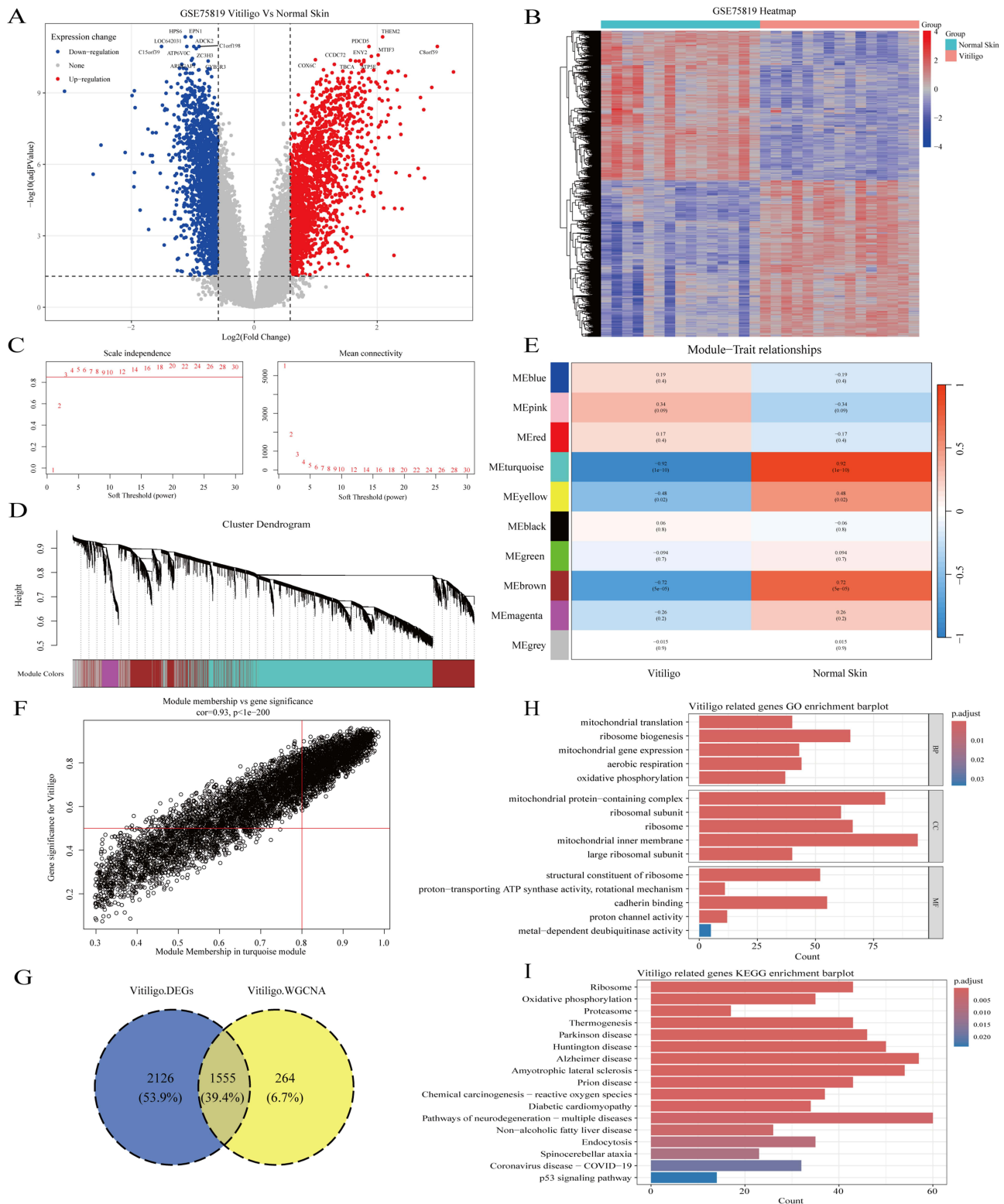


**Figure 1** Vitiligo-related features and functions. **(A)** Volcano plot of differential expression analysis of GSE75819. **(B)** Heatmap of differential expression analysis of GSE75819. **(C)** WGCNA screening for optimal softPower in GSE75819. **(D)** Dendrogram of co-expression network after merging modules in GSE75819. **(E)** Heatmap of correlation between modules and phenotypes. **(F)** Scatterplot for the screening of genes that satisfy  $MM > 0.8$  and  $GS > 0.5$  within the turquoise module. **(G)** Venn plot of DEGs and co-expressed genes of vitiligo with an intersection. **(H)** Barplot of GO enrichment analysis of vitiligo-related genes. **(I)** Barplot of KEGG enrichment analysis of vitiligo-related genes.

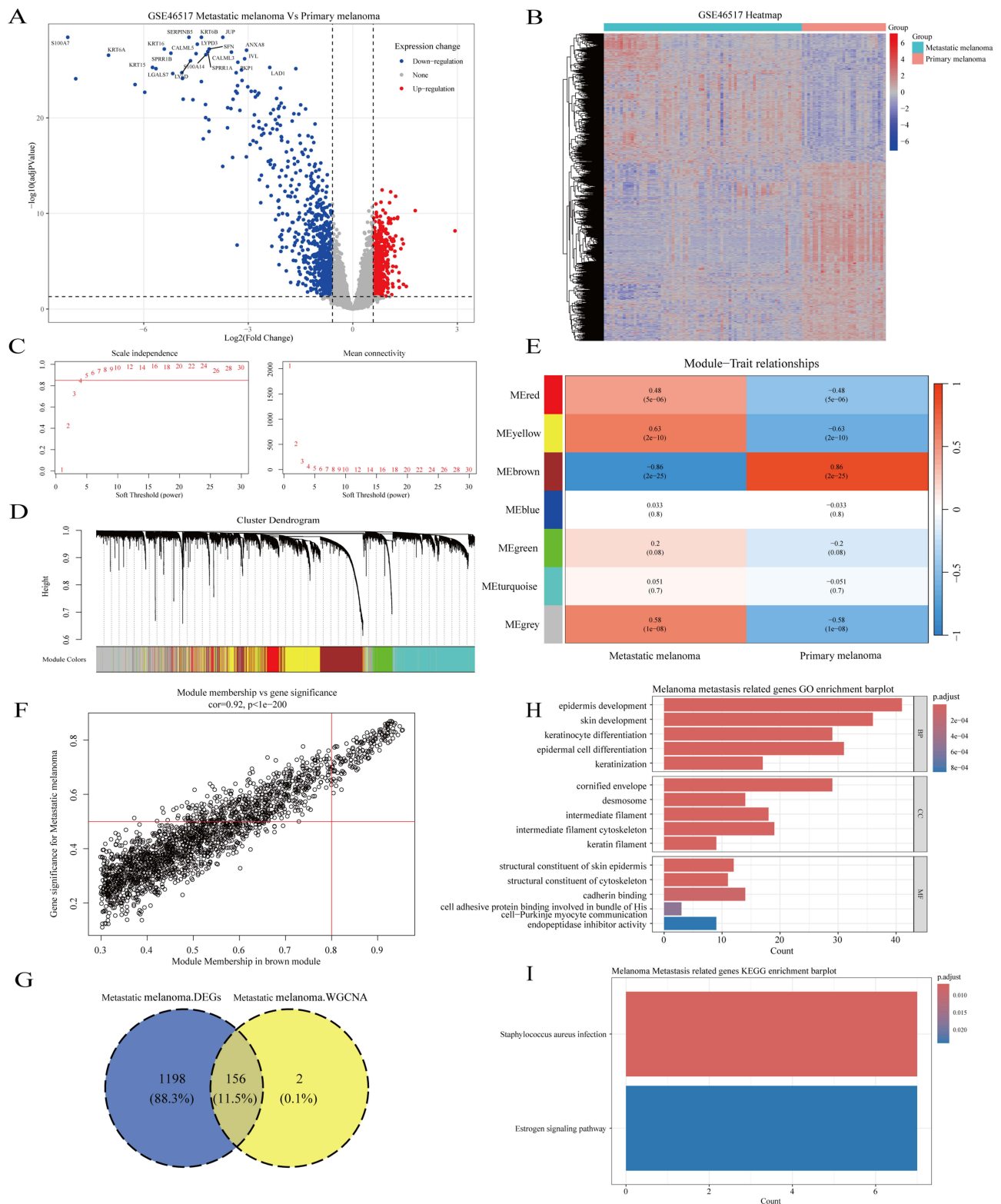


**Figure 2** Metastatic melanoma-related features and functions. **(A)** Volcano plot of differential expression analysis of GSE46517. **(B)** Heatmap of differential expression analysis of GSE46517. **(C)** WGCNA screening for optimal softPower in GSE46517. **(D)** Dendrogram of co-expression network after merging modules in GSE46517. **(E)** Heatmap of correlation between modules and phenotypes. **(F)** Scatterplot for the screening of genes that satisfy MM > 0.8 and GS > 0.5 within the brown module. **(G)** Venn plot of DEGs and co-expressed genes of metastatic melanoma with an intersection. **(H)** Barplot of GO enrichment analysis of melanoma metastasis-related genes. **(I)** Barplot of KEGG enrichment analysis of melanoma metastasis-related genes.

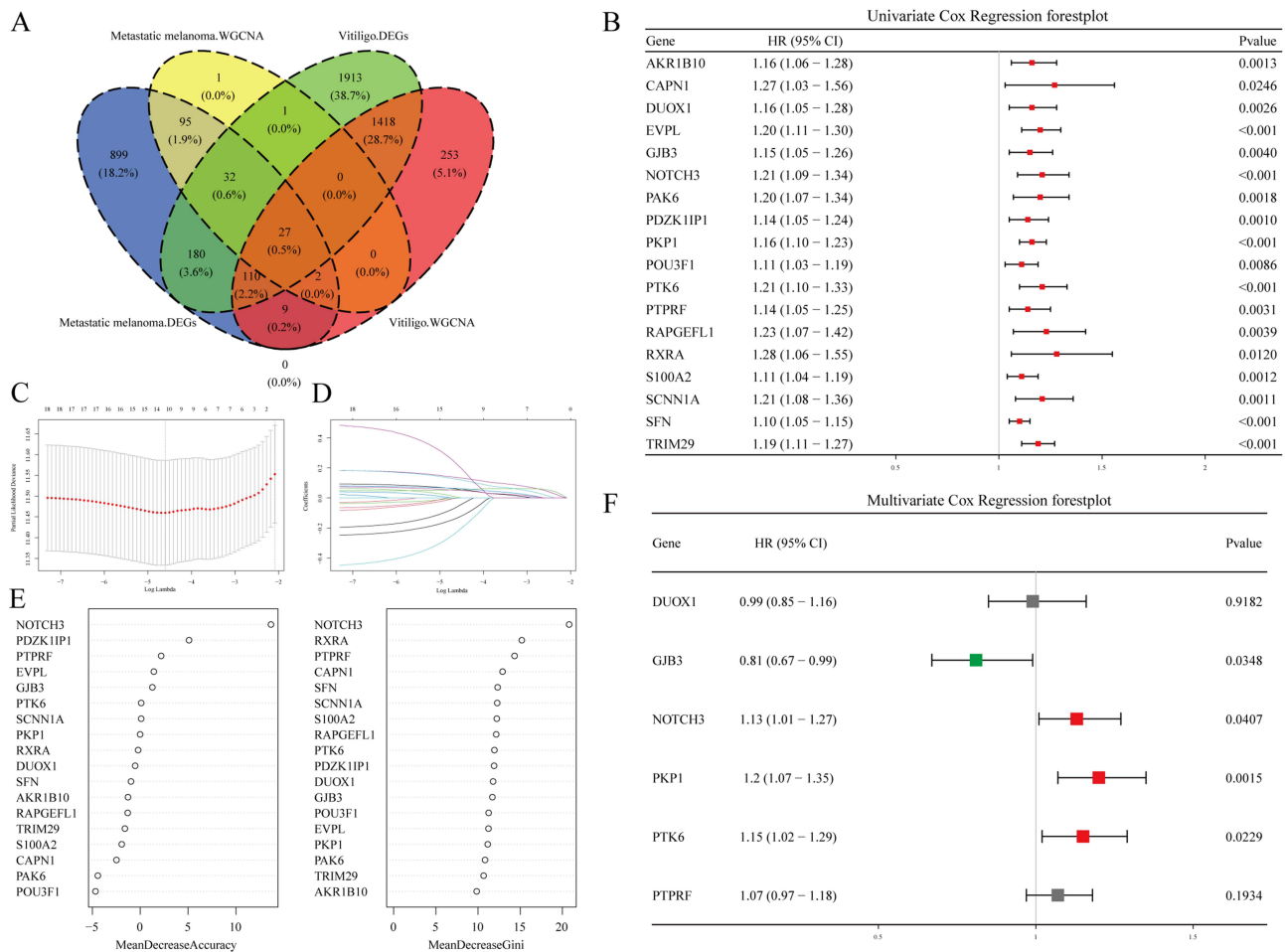


**Figure 3** Construction of prognostic models by machine learning. **(A)** Venn plot of DEGs and co-expressed genes from vitiligo and metastatic melanoma, respectively with an intersection. **(B)** Univariate Cox regression forest plot. **(C and D)** The LASSO-COX method. **(E)** The RF algorithm with genes ranked based on the MDA and MDG. **(F)** Multivariate Cox regression forest plot.

cohort, while the external validation set was derived from 214 samples from GSE65904. The risk score formula for the model was as follows:

$$\begin{aligned}
 Riskscore = & -0.007987585 \times Expr(DUOX1) - 0.209548840 \times Expr(GJB3) + 0.122011769 \times Expr(NOTCH3) \\
 & + 0.184300231 \times Expr(PKP1) + 0.138353624 \times Expr(PTK6) + 0.065018303 \times Expr(PTPRF)
 \end{aligned}$$

Among the 6 hub VMRGs, *GJB3*, *NOTCH3*, *PKP1*, and *PTK6* were independently associated with prognosis (Figure 3F), with *GJB3* being a protective factor ( $HR < 1$ ,  $p < 0.05$ ) and *NOTCH3*, *PKP1*, and *PTK6* being risk factors ( $HR > 1$ ,  $p < 0.05$ ).

### Validation of the Prognostic Model

The training set was divided into two groups, designated as high-risk ( $n = 299$ ) and low-risk ( $n = 151$ ), based on the calculated optimal cutoff value of 0.796. Kaplan-Meier analysis revealed that patients in the high-risk group exhibited a significantly poorer overall survival ( $p < 0.05$ ; Figure 4A). The AUC values of the 1-, 3-, and 5-year time points ROC curves were 0.718, 0.667, and 0.646, respectively. These values indicate that the prognostic model maintained good sensitivity and specificity over long latitudes (Figure 4B). To assess the reliability of the prognostic model, risk scores for the external validation set were calculated using the same risk score formula. In the external validation set, the high-risk ( $n = 160$ ) and low-risk ( $n = 50$ ) groups were divided based on the optimal cutoff value of 2.93. Kaplan-Meier analysis also demonstrated that the high-risk group exhibited a poorer prognosis ( $p < 0.05$ ; Figure 4D). The 1-, 3-, and 5-year

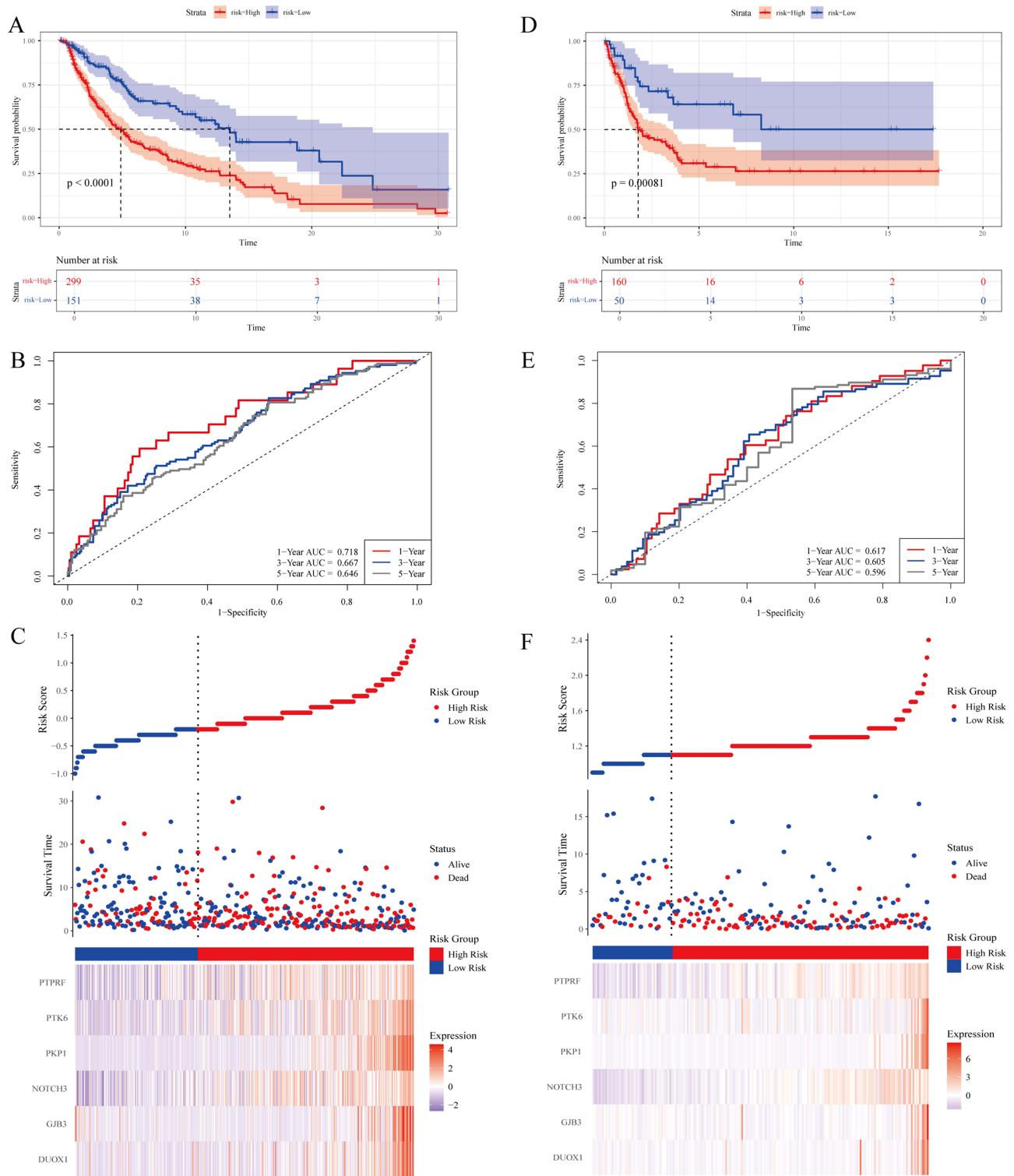


**Figure 4** Validation of the prognostic model. (A) Kaplan-Meier plots in the training set (TCGA-SCKM). (B) ROC curves in the training set (TCGA-SCKM). (C) The distribution of risk score, associated survival data, and expression of the hub VMRGs in the training set (TCGA-SCKM). (D) Kaplan-Meier plots in the external validation set (GSE65904). (E) ROC curves in the external validation set (GSE65904). (F) The distribution of risk score, associated survival data, and expression of the hub VMRGs in the external validation set (GSE65904).

time points ROC (AUC) for the external validation set were 0.617, 0.605, and 0.596, respectively (Figure 4E). The distributions of risk score, survival status, and expression levels of the hub VMRGs for the training set and external validation set were illustrated in Figure 4C and F, respectively. Ultimately, the subgroups were delineated according to age, sex, T, N, and M stage in the TCGA-SKCM cohort. Kaplan-Meier analyses revealed that the high-risk group had a lower overall survival rate than the low-risk group, except for the M1 subgroup (Supplementary Figure S3A–J). It's worth noting that GSE65904 includes more advanced-stage patients, potentially limiting model generalizability. It is of note that the model demonstrated prognostic capability, indicating potential use in predicting melanoma progression in patients.

## Nomogram Construction and Validation Based on Risk Score

To ascertain whether the risk score is an independent prognostic factor for melanoma patients, univariate and multivariate Cox regression were performed on the TCGA-SKCM cohort, respectively. The univariate Cox regression (Figure 5A) revealed that the risk score, age, T4, N1, N3 and M were correlated with prognosis ( $HR > 1, p < 0.05$ ). Meanwhile, in the multivariate Cox regression (Figure 5B), the risk score, age, T4, N1, and N3 were identified as independent risk factors ( $HR > 1, p < 0.05$ ). By integrating the risk score with all clinicopathological features, we developed a nomogram to facilitate the optimal utilization of the risk score in a clinical setting. Figure 5C presented a nomogram and a specific example of use. The calibration plot demonstrated that the predictive outcomes of the nomogram were in close alignment with the ideal model (Figure 5D). Furthermore, the ROC curve substantiated the favorable predictive capacity of the nomogram at the 1-, 3-, and 5-year time points (Figure 5E). The DCA illustrated that the nomogram exhibited superior clinical utility at the 3- and 5-year time points (Figure 5F). The aforementioned results indicated that the nomogram developed on the basis of risk score exhibited superior predictive performance in relation to the prognosis of melanoma patients.

## Functional Annotations for Hub VMRGs Based on Risk Score

To understand the survival differences between the high-risk and low-risk groups, we identified a total of 583 DEGs (Figure 6A). Of these, 491 were upregulated and 92 were downregulated ( $FDR < 0.05$  and  $|\log_2 \text{fold change}| > 0.585$ ). Subsequently, the identified DEGs were subjected to GO and KEGG enrichment analyses. The GO analyses indicated that these DEGs were predominantly associated with skin and epidermal development and differentiation (Figure 6B). KEGG was primarily associated with pathways such as the cytoskeleton in muscle cells and ECM-receptor interaction, as illustrated in Figure 6C. Subsequently, GSEA based on Hallmark gene sets (Figure 6D) demonstrated that epithelial mesenchymal transition (EMT), angiogenesis, and Notch signaling pathways were significantly up-regulated, while IL6/JAK/STAT3 signaling and interferon alpha response were down-regulated. These findings may contribute to the poor prognosis observed in the high-risk group relative to the low-risk group.

## The Landscape of the Immunological Properties in Melanoma

The infiltration of immune cells exerts a significant influence on tumor development. The outcomes of the CIBERSORT algorithm, as illustrated in Figure 7A and B, indicated that patients in the high-risk group exhibited elevated proportions of T cells CD4 memory resting, macrophages M0 and M2, while the proportions of plasma cells, T cells CD8, T cells CD4 memory activated, T cells gamma delta, and macrophages M1 were diminished, in comparison to the low-risk group. The ESTIMATE results indicated that the high-risk group exhibited lower immune scores and no difference in stromal scores (Figure 7C and D). This indicates that patients in the high-risk group may exhibit a suppressive cellular immune response. The vast majority of ICGs were highly expressed in low-risk groups, indicating that immune checkpoint blockade (ICB) is more beneficial (Figure 7E). Pearson correlation analyses were conducted for the hub VMRGs, risk score, immune cells, and ICGs (Figure 7F and G). The findings revealed that the *NOTCH3* expression pattern in immune cells was more aligned with the high-risk group. The other hub VMRGs and risk score showed a negative correlation with most ICGs.

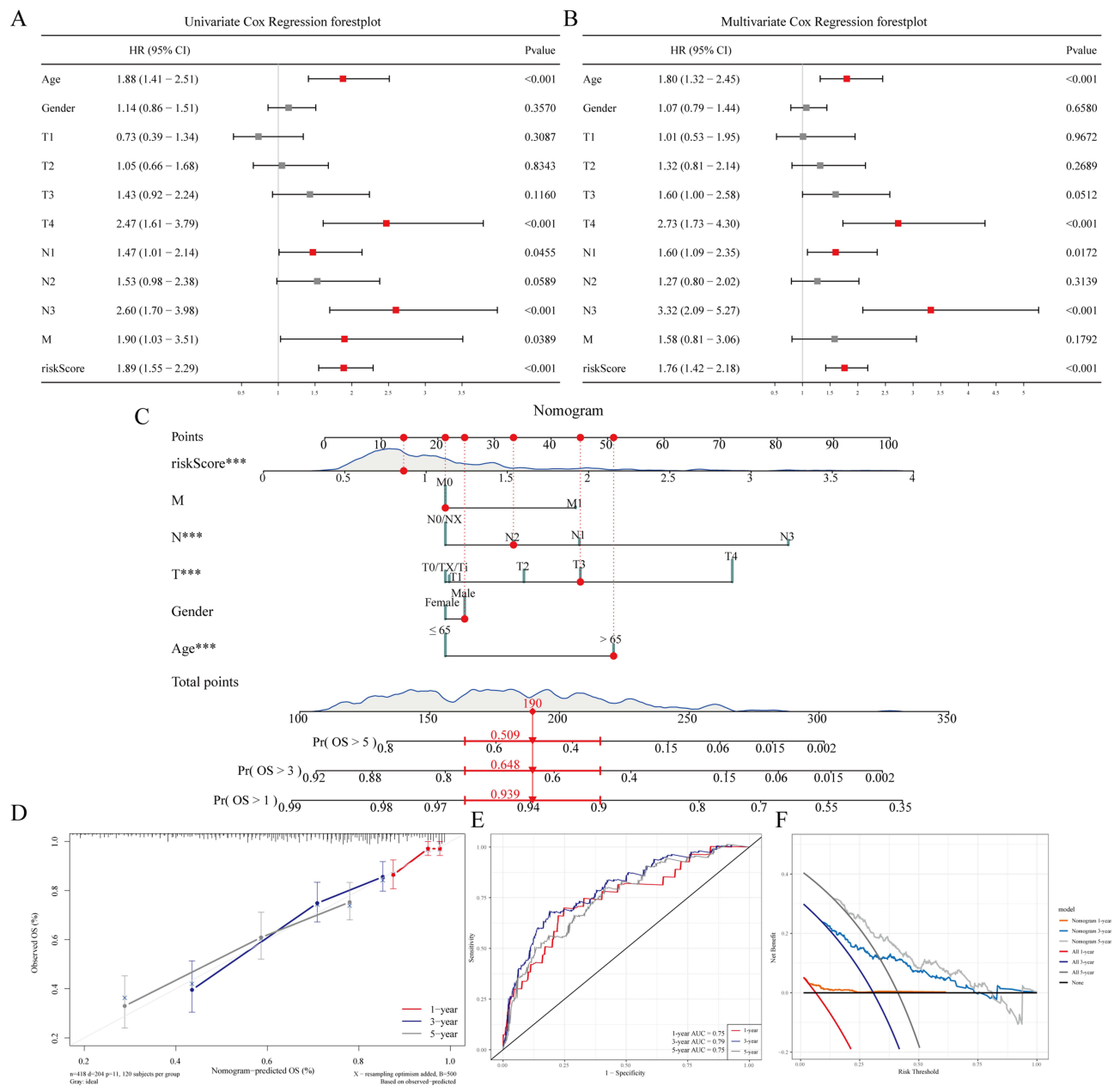


**Figure 5** Nomogram construction and validation. **(A)** Univariate Cox regression forest plot. **(B)** Multivariate Cox regression forest plot. **(C)** A nomogram model was employed to predict 1-, 3-, and 5-year time points survival probabilities for melanoma patients. The red text represented an example sample's points on each item as well as survival probabilities at different time points. **(D)** Calibration curves. **(E)** ROC curves. **(F)** Decision curve analysis plot. \*\*\*p < 0.0001.

### Expression Characteristics of Hub VMRGs and Association with Prognostic Features

The expression characteristics of the hub VMRGs in the GSE75819, GSE46517 and TCGA-SKCM cohort were further investigated (Figure 8A–C). The results indicate that hub VMRGs were less expressed in patients with vitiligo and post-metastatic melanoma, exhibiting a consistent pattern. Conversely, they were more highly expressed in the high-risk group, suggesting a worse prognosis. Kaplan-Meier plots (Figure 8D–I) indicated that high expression of all hub VMRGs except for *GJB3* predicted a worse prognosis. Furthermore, there was a significant association between overall survival and *NOTCH3*, *PKP1*, and *PTK6* ( $p < 0.05$ ). Finally, we additionally validated in the GSE8401<sup>22</sup> (52 metastatic melanoma samples vs 31 primary melanoma samples, Figure 8J) and GSE7553<sup>23</sup> (40 metastatic melanoma samples vs 14 primary

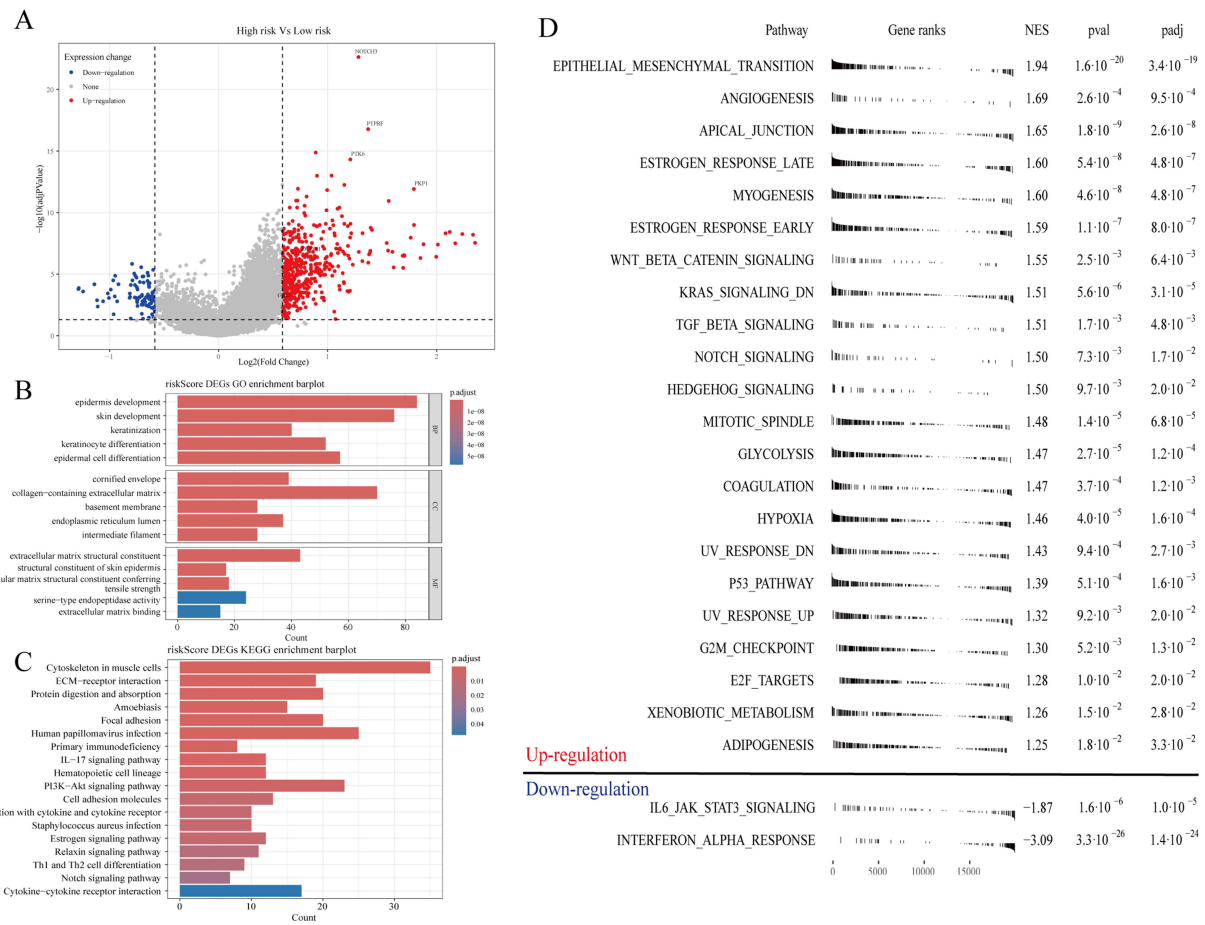


**Figure 6** Functional annotations for hub VMRGs based on risk score. **(A)** Volcano plot of differential expression analysis in the TCGA-SKCM cohort. **(B)** Barplot of GO enrichment analysis of genes associated with the risk score. **(C)** Barplot of KEGG enrichment analysis of genes associated with risk scores. **(D)** GSEA of DEGs in high- and low-risk groups.

melanoma samples, [Figure 8K](#)) datasets for expression levels of hub VMRGs, and the results and trends were consistent with our previous findings, suggesting that our results were reliable and stable.

## Validation of Cell Specificity of Hub VMRGs by scRNA-Seq

Following quality control of the GSE215120 dataset, a total of 23,882 single cells originating from cutaneous melanoma samples were obtained ([Supplementary Figure S4A](#) and [B](#)). The top 2000 HVGs were selected for inclusion in the PCA ([Supplementary Figure S4C](#)), and the top 20 principal components were selected for UMAP reduction ([Supplementary Figure S4D](#)). [Supplementary Figure S4E](#) showed UMAP plots before and after batch effect removal. Following an evaluation of alternative resolution values, 0.5 was selected as the optimal value for clustering, resulting in the identification of 16 clusters ([Supplementary Figure S4F](#) and [Figure 9A](#)). The clusters were ultimately annotated in accordance with well-known cell marker genes ([Figure 9A](#) and [B](#)). The AUCell scores of hub VMRGs were markedly concentrated on fibroblast cells ([Figure 9C](#) and [D](#)). The analysis of cell communication revealed that the fibroblast cells exhibited the strongest outgoing interaction strength ([Figure 9E](#) and [F](#)). To this end, we conducted further investigation into the interaction between fibroblast cells and melanoma cells. Our findings revealed a significant interaction between the two cells, with COL1A1/COL1A2/COL6A1/COL6A2-CD44 being the most pronounced ([Figure 9G](#)). Finally, we investigated the correlation between the hub VMRGs and these genes ([Figure 9H](#)). The Pearson correlation demonstrated that *NOTCH3* exhibited a significant positive correlation with *COL1A1*, *COL1A2*, *COL6A1*, and *COL6A2* ( $p < 0.05$ ).

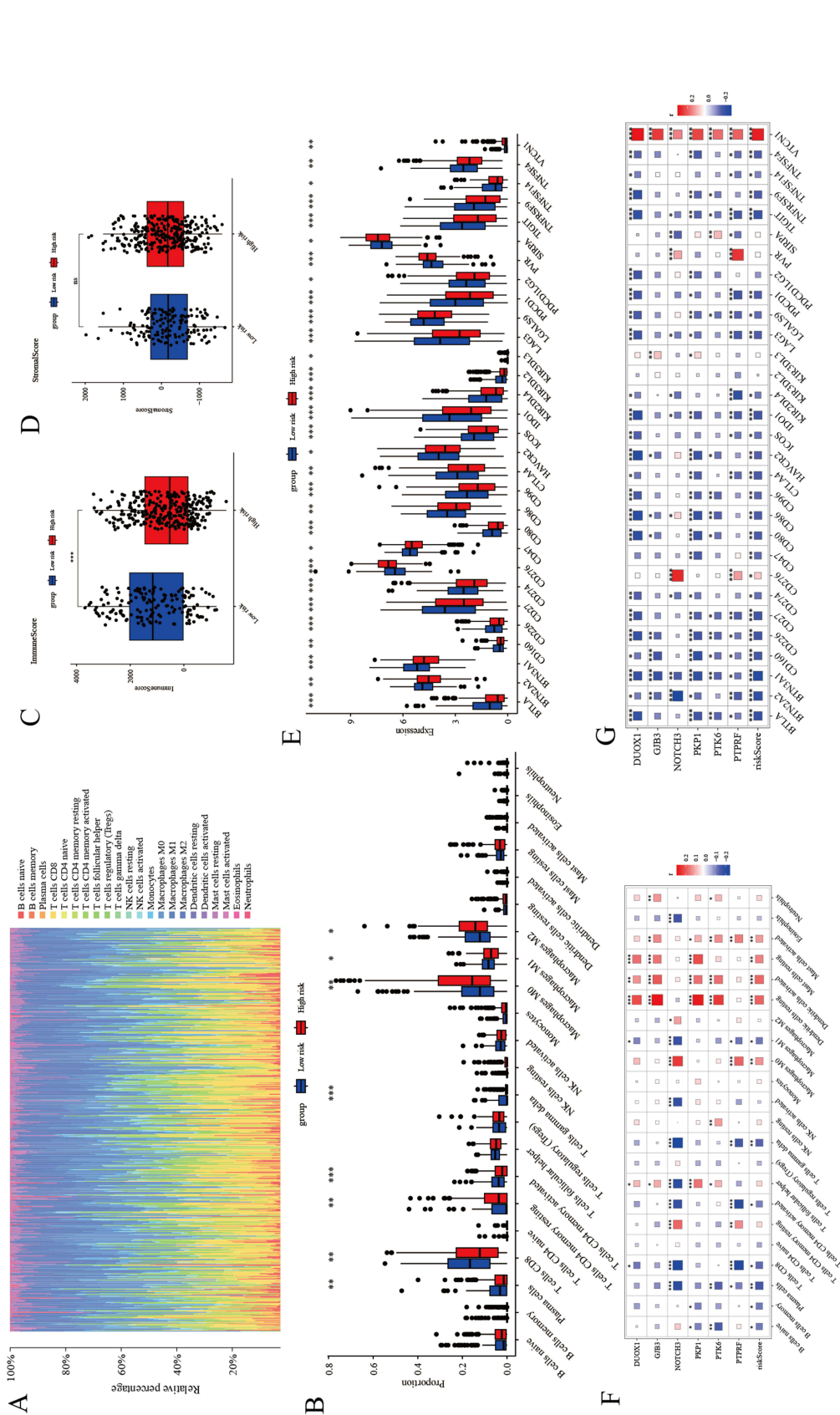


**Figure 7** The landscape of the immunological properties in melanoma. **(A)** Rainbow plot of the relative percentages of each immune cell. **(B)** Boxplot illustrates the relative distribution of immune cells between the high- and low-risk groups. **(C)** Boxplot illustrates the comparison of ImmuneScore between the high- and low-risk groups. **(D)** Boxplot of StromalScore comparisons between the high- and low-risk groups. **(E)** Boxplot illustrates the comparison of ICG expression levels between the high- and low-risk groups. **(F)** Correlation between the hub VMRGs, the risk score and the immune cells. **(G)** Correlation between the hub VMRGs, the risk score and the ICGs expression levels. \* $p < 0.05$ , \*\* $p < 0.001$ , \*\*\* $p < 0.0001$ , ns  $p > 0.05$ .

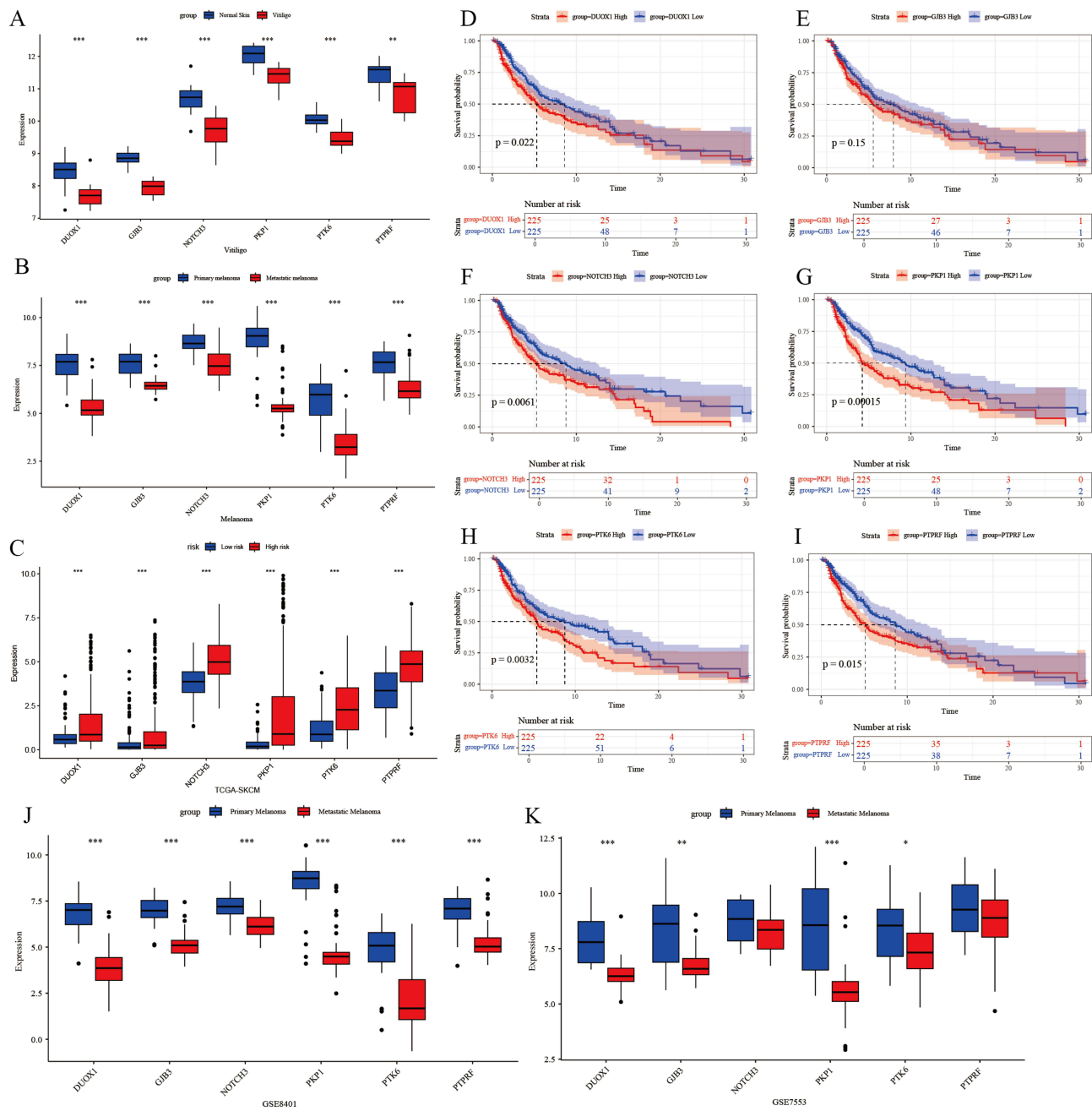


**Figure 8** Expression characteristics of hub VMRGs and association with prognostic features. (A) The expression levels of hub VMRGs in GSE75819. (B) The expression levels of hub VMRGs in GSE46517. (C) The expression levels of the hub VMRGs in the TCGA-SKCM cohort. (D–I) Kaplan-Meier plots demonstrate the correlation between the expression levels of *GJB3*, *NOTCH3*, *PKP1*, *PTK6*, and *PTPRF* in TCGA-SKCM cohort and the probability of patient survival. (J) The expression levels of hub VMRGs in GSE8401. (K) The expression levels of hub VMRGs in GSE7553. \**p* < 0.05, \*\**p* < 0.001, \*\*\**p* < 0.0001.

## Prediction of Potential Therapeutic Compounds

150 up-regulated and 92 down-regulated genes between high risk and low risk groups were used to predict small-molecule compounds in CMap database. We selected the five compounds with the lowest scores as the most promising therapeutic molecules: methyl-angolensate, byssochlamic-acid, homoharringtonine, piperacillin and cephaeline (Figure 10A). The molecular docking results were shown in Figure 10B, where the lower the affinity (kcal/mol), the tighter the binding was considered to be. Unfortunately, the structure of GJB3 was not obtained. We then show specific results of NOTCH3 docking to byssochlamic-acid, methyl-angolensate, and cephaeline (Figure 10C–E).

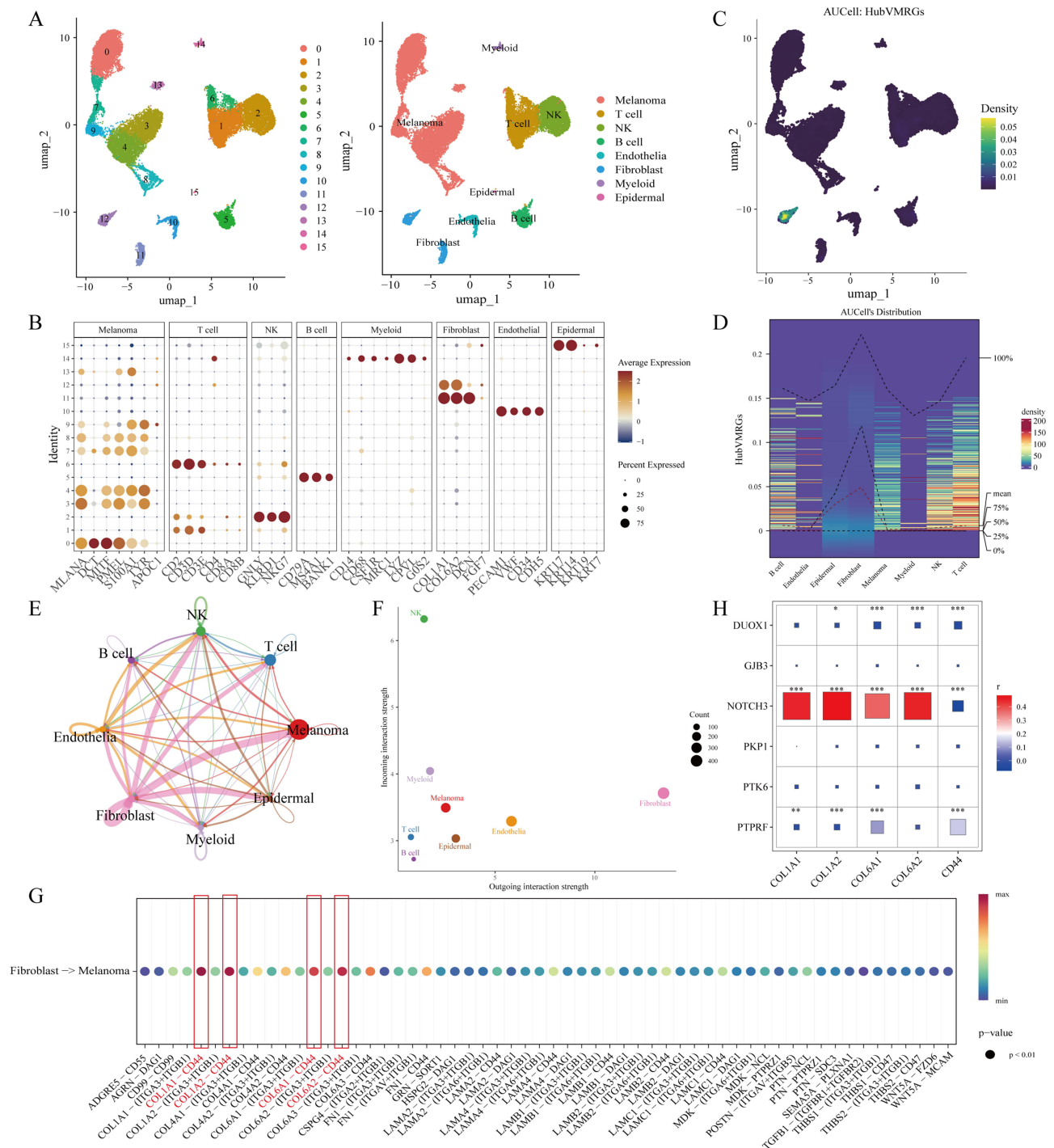


**Figure 9** scRNA-seq analysis. **(A)** UMAP reduction plot, from left to right: colored by clusters; cell types. **(B)** Heatmap of cell marker genes expression in different clusters and association with cell type. **(C)** AUCell score of hub VMRGs in the UMAP reduction plot. **(D)** The distribution of the AUCell score of hub VMRGs. **(E)** Circle plot of signaling networks in melanoma. **(F)** Dot plot was presented to demonstrate the strength of cellular output and input communication. **(G)** Cell-cell interaction between fibroblast and melanoma. The red text and boxes highlight the strong communication strength of these ligand-receptor pairs. **(H)** Correlation between hub VMRGs and key cell-cell interaction genes. \* $p < 0.05$ , \*\* $p < 0.001$ , \*\*\* $p < 0.0001$ .

**Discussion**

Melanoma is a highly malignant tumor with a high propensity for invasion and metastasis, which collectively portend a very poor prognosis.<sup>24</sup> Despite the significant advancements that have been made in the treatment of melanoma, numerous challenges remain.<sup>25</sup> There have been numerous studies showing that patients with vitiligo have a lower risk of

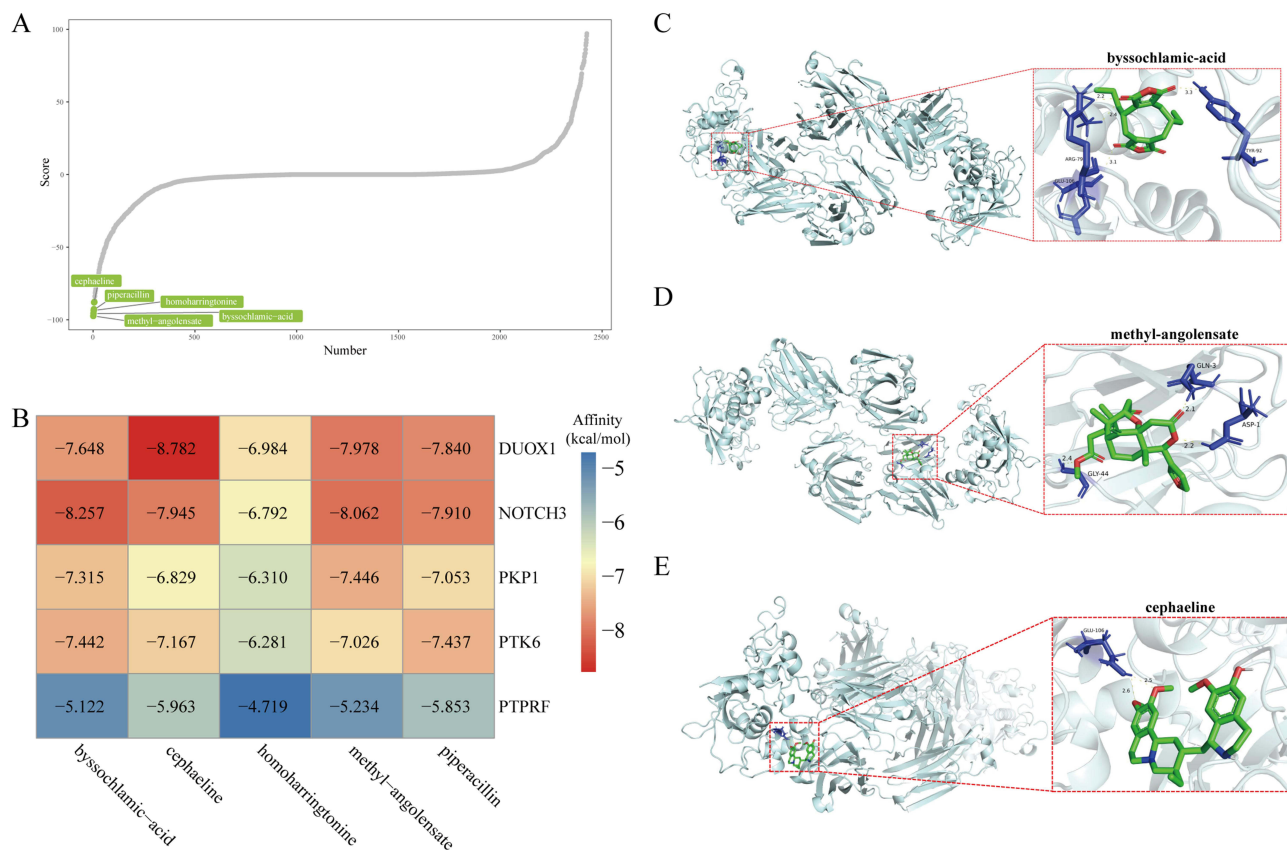


**Figure 10** Small-molecule compounds prediction and molecular docking. **(A)** Predicting results for potential therapeutic compounds by CMap database. **(B)** Heatmap of the affinity of molecular docking. **(C–E)** Detailed docking diagram of NOTCH3 docking with bissochlamic-acid, methyl-angolensate, and cephaeline, respectively.

developing melanoma and that patients with melanoma who develop vitiligo-like skin changes have a better prognosis.<sup>5–7</sup> Although the fact that the potential relationship between vitiligo and melanoma has now been elucidated in terms of humoral and cellular immunity,<sup>9</sup> there remains a paucity of research investigating the crosstalk between vitiligo and melanoma at the gene expression level, as well as studies based on vitiligo-related biomarkers.

In this study, we screened genes associated with vitiligo and metastatic melanoma combined with differential expression analysis and WGCNA. Furthermore, hub VMRGs (*DUOX1*, *GJB3*, *NOTCH3*, *PKP1*, *PTK6*, and *PTPRF*) were identified as being significantly associated with prognosis by machine learning algorithms, and validated the expression levels in independent cohorts. A prognostic model based on these genes in the TCGA-SKCM cohort was developed and also externally validated in GSE65904. The prognostic model classifies melanoma patients into high-risk and low-risk groups. The high-risk group had a worse prognosis. Consequently, A nomogram was developed to provide new insights for clinical decision-making. Finally, the immune landscape, single-cell characteristics and therapeutic compounds of melanoma patients were subjected to further investigation. Compared with previous studies,<sup>26,27</sup> this study is the first to use multi-omics and machine learning to integrate vitiligo data and discover Notch signaling pathway unique crosstalk mechanism.

Among the six hub VMRGs, firstly, *NOTCH3* and Notch signaling pathway may play a pivotal role in the crosstalk between vitiligo and metastatic melanoma. Vitiligo is a condition characterized by the loss of pigmentation in the skin, caused by the dysfunction or absence of melanocytes. The development and maintenance of the melanocyte lineage is dependent on Notch signaling.<sup>28</sup> Inactivation of Notch signaling eliminates melanocytes and melanocyte stem cells, resulting in severe hair pigmentation defects.<sup>29</sup> The inactivation of *NOTCH1* in vitiligo has been shown to result in the loss of epidermal and/or follicular active melanocytes<sup>30</sup> Despite the absence of prior reports associating *NOTCH3* with vitiligo, our study revealed a notable reduction in *NOTCH3* expression in vitiligo tissues relative to normal skin tissues

(Figure 8A). Conversely, aberrant activation of the Notch signaling pathway has been observed to promote melanoma development and metastasis. Furthermore, inhibition of the Notch signaling pathway has been demonstrated to suppress melanoma cell proliferation.<sup>31</sup> *NOTCH3* has been shown to mediate communication between melanoma cells and endothelial cells, as well as tumor cell migration.<sup>32</sup> In our study, *NOTCH3* was found to be highly expressed in the high-risk group (Figure 8C), indicating a worse prognosis (Figure 8F). Furthermore, there was a strong correlation between *NOTCH3* expression and immunosuppression (Figure 7F and G). GSEA demonstrated that the Notch signaling pathway was up regulated in the high-risk group (Figure 6D). In conclusion, there is evidence to suggest that *NOTCH3* plays a pivotal role in the pathogenesis of both vitiligo and melanoma.

Additionally, other hub VMRGs are also linked to the development and progression of cancers. *PKPI* has significant effects on melanoma cell proliferation, migration, invasion and cell cycle<sup>33</sup> *PTK6* has been identified as a pro-carcinogenic factor in a number of cancer types, including breast cancer<sup>34</sup> and prostate cancer.<sup>35</sup> Additionally, there is evidence to suggest that it may play a role in the development of metastatic melanoma.<sup>36</sup> *GJB3* has been demonstrated to promote liver metastasis in pancreatic cancer.<sup>37</sup> The potential of this marker to be a new melanoma marker was first reported in 2019, but further studies are currently lacking.<sup>38</sup> It was observed that *DUOX1* exerts a dual role in melanoma, inhibiting proliferation but promoting metastasis.<sup>39</sup> *PTPRF* has manifested inhibitory effects against gastric adenocarcinoma<sup>40</sup> and breast cancer,<sup>41</sup> yet the mechanism of action in melanoma remains opaque.

The infiltration of immune cells represents a pivotal mechanism in the progression of tumors. The proportion of plasma cells, CD8 T cells, memory-activated CD4 T cells, and gamma delta T cells infiltrated in the high-risk group of patients was found to be significantly reduced (Figure 7B), indicating that T-cell immunity were suppressed in the high-risk group. We observed a rise in M2 macrophage infiltration and a lower degree of M1 macrophage infiltration in the high-risk group (Figure 7B). These results suggest that tumors in the high-risk group have a greater tumor-associated macrophage (TAM) infiltration. ICB has played a significant role in the treatment of melanoma in recent years. A comparison of the expression levels of ICGs between high- and low-risk groups revealed that the majority of ICGs were relatively highly expressed in the low-risk group (Figure 7E), indicating that the low-risk group may potentially derive greater benefit from ICB.

In recent years, the development of scRNA-seq techniques has facilitated a deeper understanding of cellular composition and interactions within tumors. *CD44* is a critical mediator in the EMT process observed in tumor development.<sup>42</sup> Our findings indicate that hub VMRGs may play a role in melanoma proliferation and metastasis by influencing fibroblasts to promote EMT (Figure 9C–G). The results of the correlation analysis indicated a significant and positive correlation between *NOTCH3* and *COL1A1*, *COL1A2*, *COL6A1*, and *COL6A2*, which are collagen genes associated with fibroblasts.<sup>43</sup>

Finally, we found that methyl-angolensate, byssochlamic-acid, homoharringtonine, piperacillin and cephaeline may be potential therapeutic compounds for targeting hub VMRGs based on Cmap database and molecular docking. In these compounds, homoharringtonine can inhibit melanoma cell proliferation by inducing DNA damage, apoptosis and G2/M cell cycle arrest.<sup>44</sup> Meanwhile, it has been indicated to inhibit the NOTCH/MYC pathway,<sup>45</sup> which is consistent with our results. Although the remaining compounds are not reported to be directly associated with melanoma, they are closely related to tumor therapy and require further research in the future. Taken together, our results suggest that NOTCH3 may be a new potential therapeutic target for the treatment of melanoma.

It should be noted that our study is not without limitations. We have developed a prognostic model using publicly available data. While external validation indicates a degree of robustness, further clinical validation is required to confirm its generalizability and to address the possibility of overfitting to specific sample sets.

## Conclusions

We firstly investigated the crosstalk mechanisms between vitiligo and metastatic melanoma by integrating multi-omics and machine learning. Prognostic model and nomogram were constructed from hub genes (*DUOX1*, *GJB3*, *NOTCH3*, *PKPI*, *PTK6* and *PTPRF*), which was able to accurately stratify risk for melanoma patients. NOTCH3 and Notch signaling pathway may play a pivotal role in the crosstalk between vitiligo and metastatic melanoma, but extensive human and animal experiments are needed for further validation in the future. Finally, we predicted potential small-molecule compounds and verified the affinity of hub VMRGs by molecular docking. In conclusion, this study may provide important information to improve the prognosis of melanoma patients.

## Abbreviations

ASCO, American Society of Clinical Oncology; AUC, area under the curve; BP, biological process; CAF, cancer-associated fibroblast; CC, cellular component; CMap, The Connectivity Map; EMT, epithelial mesenchymal transition; FDR, false discovery rate; GEO, Gene Expression Omnibus; GO, gene ontology; HVGs, highly variable genes; ICB, immune checkpoint blockade; ICG, immune checkpoint gene; KEGG, Kyoto encyclopedia of genes and genomes; KM, Kaplan–Meier; LASSO, least absolute shrinkage and selection operator; MCSLC, melanoma cancer stem-like cells; MDA, MeanDecreaseAccuracy; MF, molecular function; NES, normalized enrichment score; PCA, principal component analysis; ROC, receiver operating characteristic; ROS, reactive oxygen species; TAM, tumor associated macrophage; TCGA, The Cancer Genome Atlas; UMAP, uniform manifold approximation and projection; UMIs, unique molecular identifiers; UVR, ultraviolet radiation; WGCNA, weighted gene co-expression network analysis.

## Data Sharing Statement

The datasets analyzed during the current study are available in the Gene Expression Omnibus (<https://www.ncbi.nlm.nih.gov/geo/>) and The Cancer Genome Atlas (<https://portal.gdc.cancer.gov/>) databases.

## Ethics Statement

This study utilized publicly available data from open access databases and did not involve any sensitive personal information or commercial interests. According to Article 32 of the Measures for Ethical Review of Life Science and Medical Research Involving Human Beings adopted by the National Science and Technology Ethics Committee of the People's Republic of China, ethical review can be exempted.

## Author Contributions

All authors made a significant contribution to the work reported, whether that is in the conception, study design, execution, acquisition of data, analysis and interpretation, or in all these areas; took part in drafting, revising or critically reviewing the article; gave final approval of the version to be published; have agreed on the journal to which the article has been submitted; and agree to be accountable for all aspects of the work.

## Funding

This work was supported by Sichuan Provincial Administration of Traditional Chinese Medicine [grant numbers 2023zd019]; Science and Technology Department of Sichuan Province [grant numbers 2024YFFK0165].

## Disclosure

The authors declare that they have no competing interests.

## References

- Long GV, Swetter SM, Menzies AM, Gershenwald JE, Scolyer RA. Cutaneous melanoma. *Lancet Lond Engl*. 2023;402:485–502. doi:10.1016/S0140-6736(23)00821-8
- Seth R, Agarwala SS, Messersmith H, et al. Systemic therapy for melanoma: ASCO guideline update. *J Clin Oncol off J Am Soc Clin Oncol*. 2023;41:4794–4820. doi:10.1200/JCO.23.01136
- Chang C, Murzaku EC, Penn L, et al. More skin, more sun, more tan, more melanoma. *Am J Public Health*. 2014;104:e92–99. doi:10.2105/AJPH.2014.302185
- Ascierto PA, McArthur GA. Checkpoint inhibitors in melanoma and early phase development in solid tumors: what's the future? *J Transl Med*. 2017;15:173. doi:10.1186/s12967-017-1278-5
- Paradisi A, Tabolli S, Didona B, Sobrino L, Russo N, Abeni D. Markedly reduced incidence of melanoma and nonmelanoma skin cancer in a nonconcurrent cohort of 10,040 patients with vitiligo. *J Am Acad Dermatol*. 2014;71:1110–1116. doi:10.1016/j.jaad.2014.07.050
- Teulings HE, Overkamp M, Ceylan E, et al. Decreased risk of melanoma and nonmelanoma skin cancer in patients with vitiligo: a survey among 1307 patients and their partners. *Br J Dermatol*. 2013;168:162–171. doi:10.1111/bjd.12111
- Teulings H-E, Limpens J, Jansen SN, et al. Vitiligo-like depigmentation in patients with stage III-IV melanoma receiving immunotherapy and its association with survival: a systematic review and meta-analysis. *J Clin Oncol off J Am Soc Clin Oncol*. 2015;33:773–781. doi:10.1200/JCO.2014.57.4756
- Frisoli ML, Essien K, Harris JE. Vitiligo: mechanisms of pathogenesis and treatment. *Annu Rev Immunol*. 2020;38:621–648. doi:10.1146/annurev-immunol-100919-023531

9. Failla CM, Carbone ML, Fortes C, Pagnanelli G, D'Atri S. Melanoma and vitiligo: in good company. *Int J Mol Sci.* 2019;20:5731. doi:10.3390/ijms20225731
10. Fishman P, Azizi E, Shoenfeld Y, et al. Vitiligo autoantibodies are effective against melanoma. *Cancer.* 1993;72:2365–2369. doi:10.1002/1097-0142(19931015)72:8<2365::aid-cnrc2820720812>3.0.co;2-g
11. Baysoy A, Bai Z, Satija R, Fan R. The technological landscape and applications of single-cell multi-omics. *Nat Rev Mol Cell Biol.* 2023;24:695–713. doi:10.1038/s41580-023-00615-w
12. Reel PS, Reel S, Pearson E, Trucco E, Jefferson E. Using machine learning approaches for multi-omics data analysis: a review. *Biotechnol Adv.* 2021;49:107739. doi:10.1016/j.biotechadv.2021.107739
13. Singh A, Gotherwal V, Junni P, et al. Mapping architectural and transcriptional alterations in non-lesional and lesional epidermis in vitiligo. *Sci Rep.* 2017;7(1):9860. doi:10.1038/s41598-017-10253-w
14. Kabbarah O, Nogueira C, Feng B, et al. Integrative genome comparison of primary and metastatic melanomas. *PLoS One.* 2010;5:e10770. doi:10.1371/journal.pone.0010770
15. Cirenajwis H, Ekedahl H, Lauss M, et al. Molecular stratification of metastatic melanoma using gene expression profiling: prediction of survival outcome and benefit from molecular targeted therapy. *Oncotarget.* 2015;6:12297–12309. doi:10.18632/oncotarget.3655
16. Ritchie ME, Phipson B, Wu D, et al. limma powers differential expression analyses for RNA-sequencing and microarray studies. *Nucleic Acids Res.* 2015;43:e47. doi:10.1093/nar/gkv007
17. Wu T, Hu E, Xu S, et al. clusterProfiler 4.0: a universal enrichment tool for interpreting omics data. *Innov Camb Mass.* 2021;2:100141. doi:10.1016/j.xinn.2021.100141
18. Subramanian A, Tamayo P, Mootha VK, et al. Gene set enrichment analysis: a knowledge-based approach for interpreting genome-wide expression profiles. *Proc Natl Acad Sci U S A.* 2005;102:15545–15550. doi:10.1073/pnas.0506580102
19. Chen B, Khodadoust MS, Liu CL, Newman AM, Alizadeh AA. Profiling tumor infiltrating immune cells with CIBERSORT. *Methods Mol Biol Clifton NJ.* 2018;1711:243–259. doi:10.1007/978-1-4939-7493-1\_12
20. Zhang C, Shen H, Yang T, et al. A single-cell analysis reveals tumor heterogeneity and immune environment of acral melanoma. *Nat Commun.* 2022;13:7250. doi:10.1038/s41467-022-34877-3
21. Du L, Geng C, Zeng Q, et al. Dockey: a modern integrated tool for large-scale molecular docking and virtual screening. *Brief Bioinform.* 2023;24:bbad047. doi:10.1093/bib/bbad047
22. Xu L, Shen SS, Hoshida Y, et al. Gene expression changes in an animal melanoma model correlate with aggressiveness of human melanoma metastases. *Mol Cancer Res.* 2008;6:760–769. doi:10.1158/1541-7786.MCR-07-0344
23. Riker AI, Enkemann SA, Fodstad O, et al. The gene expression profiles of primary and metastatic melanoma yields a transition point of tumor progression and metastasis. *BMC Med Genomics.* 2008;1:13. doi:10.1186/1755-8794-1-13
24. Whiteman DC, Green AC, Olsen CM. The growing burden of invasive melanoma: projections of incidence rates and numbers of new cases in six susceptible populations through 2031. *J Invest Dermatol.* 2016;136:1161–1171. doi:10.1016/j.jid.2016.01.035
25. Berk-Krauss J, Stein JA, Weber J, Polsky D, Geller AC. New systematic therapies and trends in cutaneous melanoma deaths among US whites, 1986–2016. *Am J Public Health.* 2020;110:731–733. doi:10.2105/AJPH.2020.305567
26. Zhang Y, Xie A, Wang D, Deng W. Novel prognostic markers for skin cutaneous melanoma. *Clin Cosmet Invest Dermatol.* 2024;17:2615–2625. doi:10.2147/CCID.S486679
27. Wang X, Yang X, Zhang Y, et al. Fatty acid metabolism-related lncRNAs are potential biomarkers for predicting prognoses and immune responses in patients with skin cutaneous melanoma. *Clin Cosmet Invest Dermatol.* 2023;16:3595–3614. doi:10.2147/CCID.S417805
28. Diao J-S, Zhang X, Xia W-S, et al. Aberrant Notch signaling: a potential pathomechanism of vitiligo. *Med Hypotheses.* 2009;73:70–72. doi:10.1016/j.mehy.2009.02.003
29. Moriyama M, Osawa M, Mak -S-S, et al. Notch signaling via Hes1 transcription factor maintains survival of melanoblasts and melanocyte stem cells. *J Cell Biol.* 2006;173:333–339. doi:10.1083/jcb.200509084
30. Seleit I, Bakry OA, Abdou AG, Dawoud NM. Immunohistochemical expression of aberrant Notch-1 signaling in vitiligo: an implication for pathogenesis. *Ann Diagn Pathol.* 2014;18:117–124. doi:10.1016/j.anndiagpath.2014.01.002
31. Tang Y, Cao Y. SOX10 knockdown inhibits melanoma cell proliferation via notch signaling pathway. *Cancer Manag Res.* 2021;13:7225–7234. doi:10.2147/CMAR.S329331
32. Howard JD, Moriarty WF, Park J, et al. Notch signaling mediates melanoma-endothelial cell communication and melanoma cell migration. *Pigm Cell Melanoma Res.* 2013;26:697–707. doi:10.1111/pcmr.12131
33. Yue C, Lian W, Fan Z, et al. The role of PKP1 in tumor progression in melanoma: analysis of a cell adhesion-related model. *Environ Toxicol Int J.* 2024;39:915–926. doi:10.1002/tox.24017
34. Chen Y, Qu W, Tu J, Yang L, Gui X. Prognostic impact of PTK6 expression in triple negative breast cancer. *BMC Womens Health.* 2023;23:575. doi:10.1186/s12905-023-02736-y
35. Zheng Y, Tyner AL. Context-specific protein tyrosine kinase 6 (PTK6) signalling in prostate cancer. *Eur J Clin Invest.* 2013;43:397–404. doi:10.1111/eci.12050
36. Easty DJ, Mitchell PJ, Patel K, Flørenes VA, Spritz RA, Bennett DC. Loss of expression of receptor tyrosine kinase family genes PTK7 and SEK in metastatic melanoma. *Int J Cancer.* 1997;71:1061–1065. doi:10.1002/(sici)1097-0215(19970611)71:6<1061::aid-ije24>3.0.co;2-f
37. Huo Y, Zhou Y, Zheng J, et al. GJB3 promotes pancreatic cancer liver metastasis by enhancing the polarization and survival of neutrophil. *Front Immunol.* 2022;13:983116. doi:10.3389/fimmu.2022.983116
38. D'Arcangelo D, Scatozza F, Giampietri C, Marchetti P, Facchiano F, Facchiano A. Ion channel expression in human melanoma samples: in silico identification and experimental validation of molecular targets. *Cancers.* 2019;11:446. doi:10.3390/cancers11040446
39. Pardo-Sánchez I, Ibañez-Molero S, García-Moreno D, Mulero V. Dual role of duox1-derived reactive oxygen species in melanoma. *Antioxid Basel Switz.* 2023;12:708. doi:10.3390/antiox12030708
40. Tian X, Yang C, Yang L, Sun Q, Liu N. PTPRF as a novel tumor suppressor through deactivation of ERK1/2 signaling in gastric adenocarcinoma. *Oncol Targets Ther.* 2018;11:7795–7803. doi:10.2147/OTT.S178152
41. Xu -Y-Y, Liu H, Su L, et al. PPAR $\gamma$  inhibits breast cancer progression by upregulating PTPRF expression. *Eur Rev Med Pharmacol Sci.* 2019;23:9965–9977. doi:10.26355/eurrev\_201911\_19563

42. Chen C, Zhao S, Karnad A, Freeman JW. The biology and role of CD44 in cancer progression: therapeutic implications. *J Hematol Oncol.* 2018;11:64. doi:10.1186/s13045-018-0605-5
43. De Martino D, Bravo-Cordero JJ. Collagens in cancer: structural regulators and guardians of cancer progression. *Cancer Res.* 2023;83:1386–1392. doi:10.1158/0008-5472.CAN-22-2034
44. Tang J-F, Li G-L, Zhang T, et al. Homoharringtonine inhibits melanoma cells proliferation in vitro and vivo by inducing DNA damage, apoptosis, and G2/M cell cycle arrest. *Arch Biochem Biophys.* 2021;700:108774. doi:10.1016/j.abb.2021.108774
45. Suo S, Zhao D, Li F, et al. Homoharringtonine inhibits the NOTCH/MYC pathway and exhibits antitumor effects in T-cell acute lymphoblastic leukemia. *Blood.* 2024;144:1343–1347. doi:10.1182/blood.2023023400

Clinical, Cosmetic and Investigational Dermatology

**Publish your work in this journal**

Clinical, Cosmetic and Investigational Dermatology is an international, peer-reviewed, open access, online journal that focuses on the latest clinical and experimental research in all aspects of skin disease and cosmetic interventions. This journal is indexed on CAS. The manuscript management system is completely online and includes a very quick and fair peer-review system, which is all easy to use. Visit <http://www.dovepress.com/testimonials.php> to read real quotes from published authors.

Submit your manuscript here: <https://www.dovepress.com/clinical-cosmetic-and-investigational-dermatology-journal>

**Dovepress**  
Taylor & Francis Group